ECS Journal of Solid State Science and Technology, **2** (6) M17-M21 (2013) M17
2162-8769/2013/2(6)/M17/5/$31.00 © The Electrochemical Society

Transfer-Free Selective Area Synthesis of Graphene Using Solid-State Self-Segregation of Carbon In Cu/Ni Bilayers

Hossein Sojoudi[a] and Samuel Graham[a,b,z]

[a]*Woodruff School of Mechanical Engineering, Georgia Institute of Technology, Atlanta, Georgia 30332, USA*
[b]*School of Materials Science and Engineering, Georgia Institute of Technology, Atlanta, Georgia 30332, USA*

A method for the direct synthesis of wafer-scale graphene on dielectric substrates using trace amounts of carbon found in metals is reported. Graphene films were synthesized through a single-step thermal annealing process of a Cu/Ni bilayer deposited on a SiO_2/Si and a quartz substrate in a low pressure H_2/Ar environment. No additional carbon source was provided. The Cu film partially evaporated during growth, leaving a graphene layer above and beneath the Ni film. A wet etch step allowed complete removal of the metals, resulting in continuous graphene coverage of the surface. A simple pattered synthesis of graphene was performed using this technique demonstrating the ability to control the growth of graphene to specific regions over large areas of the wafer.
© 2013 The Electrochemical Society. [DOI: 10.1149/2.016306jss] All rights reserved.

Manuscript submitted March 4, 2013; revised manuscript received April 23, 2013. Published May 7, 2013.

The deposition or synthesis of large-area, high quality graphene[1,2] is important for developing electronic, optoelectronic, and sensor technologies as well as modifying surfaces for heat transfer and mechanics applications. Epitaxial growth from single crystal SiC has been intensely researched because it yields high quality graphene films with excellent carrier mobilities.[3–5] However, the production of large area epitaxial growth on SiC has limitations due to the expense and current size of SiC substrates.[3–5] To address these challenges, several scalable techniques have been developed to deposit graphene films onto a variety of substrates. These techniques include the chemical reduction of solution deposited graphite oxide (GO),[6–10] liquid phase exfoliation and solution deposition of graphene,[11–13] and chemical vapor deposition (CVD) on metals followed by transfer.[14–18] Among these, CVD is the most viable for fabricating continuous large area graphene sheets that is limited by the size of the metal substrates and the capacity of the CVD furnace used for synthesis.[17,18] The key feature of the CVD method is the solubility of carbon in metals such as nickel or copper at the typical synthesis temperature for graphene (900–1000°C).[14,15] Upon cooling, the carbon precipitates to the surface to form graphene.[16] The source of carbon atoms can be a hydrocarbon gas,[14–18] or they can be obtained by the decomposition of a carbon containing solid[19,20] such as a polymer,[21–23] diamond,[24] C_{60}[25] or HOPG[26] in contact with the metal catalyst film.

A segregation phenomenon has been utilized to turn the trace amounts of carbon dissolved in bulk metals into graphene.[16,27] Recently, research has shown the ability to produce graphene films using this segregation method by allowing trace C found in Ni to diffuse through an outer Cu layer to form graphene. However, the graphene films found on the Cu film and required a subsequent transfer to a second substrate after synthesis in order to remove the metal layers. In general, it is difficult to transfer a pristine sheet of large area graphene without leaving significant tears or cracks on the order of tens of microns. Direct synthesis of graphene on dielectric substrates through surface catalytic decomposition of hydrocarbon precursors on thin copper films[28,29] and carbon diffusion from solid source precursors through nickel[30,31] to form graphene have also been reported recently. While these methods present a pathway to produce continuous graphene films on dielectric substrates without a transfer step, this has yet to be demonstrated. Herein, we describe an extension of the segregation approach to form graphene both on top and underneath a Cu/Ni bilayer film without the need for a transfer step. This is a fast, easy, transfer-free, and scalable method for full coverage and can lead to patterned graphene on dielectric substrates.

Experimental

Cu and Ni films were deposited on growth substrates (Si wafer coated with 300 nm of thermal oxide or quartz) using a CVC electron-beam evaporator with a pressure of $\sim 10^{-6}$ Torr. The evaporation rates for Cu and Ni were 2 and 0.5 Å/s, respectively. The key to this process is that the evaporation utilized graphite crucibles for holding the metal sources that diffuses into the metal to leave trace amounts of carbon contamination. This trace carbon was utilized as the source for the graphene growth. To grow graphene, the sample was placed inside a quartz tube and pushed into the hot zone of a growth furnace operating at 1000°C. The growth was performed under flow rates of 50 sccm H_2 and 500 sccm Ar atmosphere at a pressure around 870 mTorr for 30 minutes. Next, the sample was cooled from 1000°C to room temperature in 20 minutes under the same gas flow rate. During growth, the sacrificial copper partially diffused into the Ni and partially evaporated away due to the high homologous temperature (>0.9) and the low pressure inside the chamber,[28] leaving graphene both on top and underneath the nickel film.

Results and Discussion

A schematic of synthesis is shown in Fig. 1a. Carbon impurities were present in the evaporated Ni and Cu films. Heating the substrate inside a furnace results in migration of C atoms inside the metal films. Further heating at higher temperatures leads to formation of Ni/Cu alloy with an intermediate carbon solubility. With the lower solubility of carbon in Cu, the Cu displaces the carbon in the Ni and causes it to diffuse to the surfaces of the alloy. This results in nucleation and growth of graphene both on top of the alloy and at the interface of alloy and growth substrate. During synthesis, much of the Cu film evaporated away, leaving behind a discontinuous residual layer of Cu on the Ni/Cu alloy. To remove the metals, the samples were treated post-growth with a 30% $FeCl_3$ acid solution for an hour followed by a 10% HCl aqueous solution for 10 min prior to washing in deionized (DI) water. This process left the graphene directly on the growth substrate. Figures 1b and 1c show a typical 100 mm diameter SiO_2/Si wafer coated with a Cu (150 nm thick)/Ni (10 nm thick) bilayer before and after synthesis. Layers of graphene can be observed by the color contrast on the wafer due to light interference effects. The lightest regions in the middle of the wafer correspond to monolayer or bilayer of graphene, where the darker regions near the edge of the wafer is mostly few-layer graphene.

Time of flight secondary ion mass spectroscopy (TOF-SIMS) 5–300 was utilized to determine the carbon distribution within the bilayer metal stack prior to growth. The system can detect trace elements down to concentrations of a few parts per million with a vertical resolution of $\sim$ 2 nm and lateral resolution as small as ~300 nm. It uses a Bi primary ion source emitting 30 keV ions. Sputtering was generated by O+ ions with 500 eV to 2 keV energy. The bilayer on a SiO_2 /Si substrate composed of 100 nm thick Cu and 100 nm thick Ni was analyzed by TOF-SIMS for this purpose. The layer thicknesses used here are different than those used for growth since they were only used

[z]E-mail: sgraham@gatech.edu

Downloaded on 2013-05-16 to IP 128.61.142.206 address. Redistribution subject to ECS license or copyright; see ecsdl.org/site/terms_use

Figure 1. (a) Schematic of the graphene synthesis procedure. (b) 100 mm Si/SiO_2 wafer covered with 10 nm think Ni and 150 nm thick Cu using CVC E-beam evaporation. (c) Graphene on Si/SiO_2 (100 mm wafer) after 30 minutes of growth.

to detect the relative amounts of carbon in each layers. The thicker layers ensured that the sputtering and ionization would occur with sufficient time in each material far enough from the Cu/Ni interface and before reaching the SiO_2 surface. Figure 2 shows the intensity of detected ions versus sputtering time close to the interface of the Cu and Ni. A high intensity of Cu- ions was first detected which formed the outer layer of the Cu/Ni bilayer film. During the depth profile analysis, the carbon to copper ion intensity ratio (I_{C-}/I_{Cu-}) in this region was ∼ 3.5 E^{-4}. Further sputtering results in diminishing of the Cu intensity and the appearance of Ni. This is indicative of reaching Cu/Ni interface. Simultaneously, an increase in the intensity of C was observed. The carbon to nickel ion intensity ratio (I_{C-}/I_{Ni-}) was ∼ 7 E^{-2}. Comparing I_{C-}/I_{Ni-} with I_{C-}/I_{Cu-} indicates that the C solubility in bulk Ni is 2 orders of magnitude higher than in Cu. This is in accord with reported maximum solubility of C in Ni and Cu (2.7% vs 0.04%).[27] This distinct difference in carbon solubilities of Ni and Cu suggest that the carbon in the Ni can be displaced once alloyed with Cu.

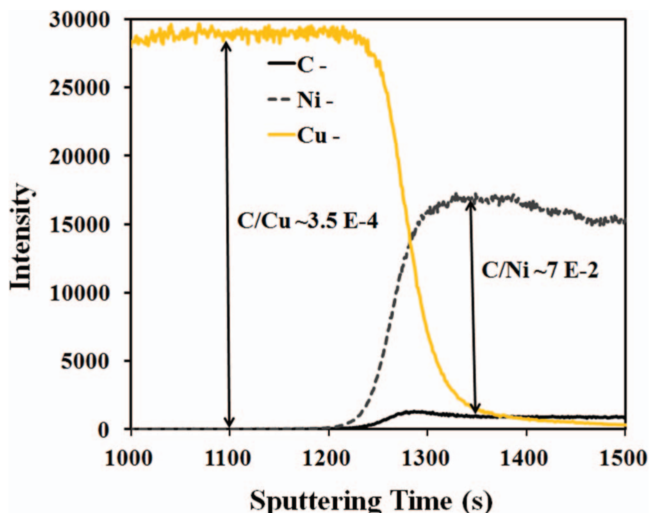

Figure 2. SIMS results show intensity of detected ions versus sputtering time indicative of 2 order of magnitude higher C solubility in Ni compare to Cu.

To further test if the C was coming from the graphite crucibles, another set of samples for growth were prepared through sputtering of Ni and Cu on SiO_2/Si substrates. The results showed that graphene was not formed in spite of using the same growth process. It is believed that the C atoms diffuse into the metal in the E-beam evaporator from the graphite crucibles used to hold the metal sources. Thus, while the differences in the solubility of C in each of the metals is important, the trace carbon appears to be an artifact of the method used to deposit the metals and the combination of these features allows for the synthesis of graphene without any additional carbon sources.

Figures 3a and 3b show optical microscope images of graphene grown on a SiO_2 substrate with 150 nm thick Cu and 10 nm thick Ni films before and after wet etching, respectively. Large regions of graphene were found on top of the Ni/Cu alloy layer, while the residual copper covered less than ∼5% of the surface. Raman spectroscopy characterization of the top graphene layer was performed by analyzing

Downloaded on 2013-05-16 to IP 128.61.142.206 address. Redistribution subject to ECS license or copyright; see ecsdl.org/site/terms_use

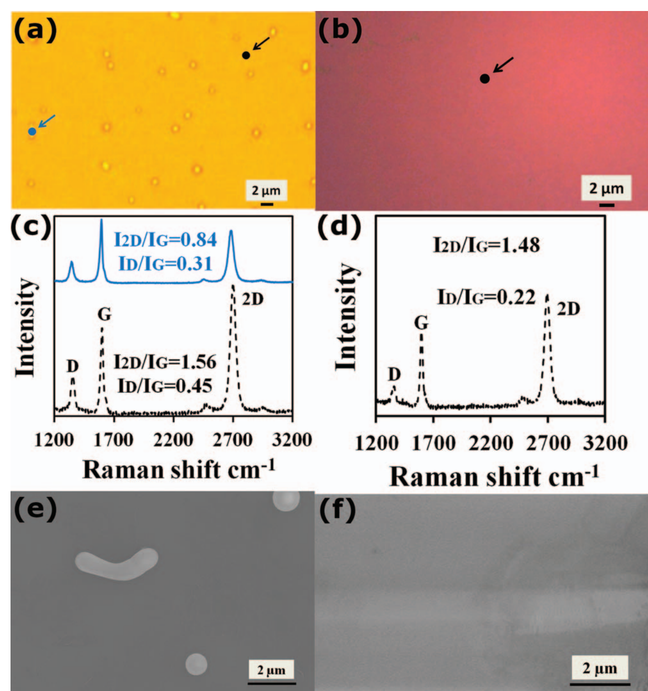

Figure 3. (a) and (b) Optical microscope image of graphene grown on Cu (150 nm)/Ni (10 nm)/SiO_2 substrate before and after wet etching treatment. (c) Raman spectra from Ni (black line) and Cu regions (blue line) showing full coverage of graphene on the sample. (d) Raman spectra from SiO_2 showing presence of graphene after wet etching of metals. (e) Secondary-electron SEM image of a graphene sample grown on Ni before wet etching. (f) In-lens SEM image of graphene on SiO_2 after wet etching of Ni and residual Cu showing presence of wrinkles.

the intensities of the D, G, and 2D Raman peaks[32] using a Jobin-Yvon micro-Raman system. All spectra were excited with visible (532 nm) laser light and collected in the backscattering configuration by using a laser, with power set below 0.5 mW to avoid laser-induced heating. A 50x objective lens was used to focus the laser on the graphene samples during the Raman measurements. All Raman peaks were fitted with Gauss-Lorentzian line shapes to determine the peak position, line width, and intensity of the D, G, and 2D Raman peaks. The Raman fingerprint for CVD graphene was confirmed by using the 2D- and G-peaks intensity ratio (I_{2D}/I_G)[17,33] and the width of the 2D-peak.[32–34] The graphene was identified in all spectra measured on samples both in the regions with and without residual Cu. Graphene on the Ni/Cu alloy had a I_{2D}/I_G of 1.56 ± 0.06 and a full width at half maximum (FWHM) of ∼ 40 ± 2 cm^{-1} suggesting a monolayer or bilayer film. In regions with residual copper, I_{2D}/I_G was ∼ 0.84 ± 0.05 and FWHM of 2D was ∼ 50 ± 3.5 cm^{-1} indicative of few-layer graphene.[17] A high D-peak intensity in copper-free areas suggests the presence of intrinsic defects in the graphene or a high density graphene domains.[33]

While wet etching was typically used to remove the metal and top graphene layers, a few samples were exposed to an oxygen plasma step prior to wet etching to ensure that the top graphene did not redeposit on the underlying substrate. This involved exposing the sample first to a Vision RIE oxygen plasma for 10–15 seconds, prior to wet etching to destroy the top layer graphene. Raman measurements performed after the oxygen plasma etching step verified that the top layer graphene was successfully removed. After wet etching, both residual Cu and Ni/Cu alloy with the top layer graphene were removed, leaving the lower layer of graphene in direct contact with the SiO_2. An I_{2D}/I_G of 1.48 ± 0.05 and a full width at half maximum (FWHM) of ∼ 41 ± 2 cm^{-1} was measured suggesting a monolayer or bilayer graphene on the SiO_2 substrate. A Zeiss Ultra60 scanning electron microscopy (SEM) imaged the graphene before and after wet etching. Figure 3e shows a SEM image of the graphene layer before wet etching. Visible regions of residual copper confirm the dewetting and evaporation of Cu. The SEM image, using an in-lens detector, in Fig. 3f clearly shows that there are wrinkle-like contrast in the continuous graphene film after wet etching. It is believed that the difference between thermal expansion coefficients of graphene and Ni induces a thermal stress during growth leads to formation of wrinkles.[27] These wrinkles have been observed in the SEM image of transferred CVD graphene films. However, the importance of our method is the lack of tears and cracks on the order of tens of microns or larger which may occur in the transfer process of CVD graphene films.

The direct synthesis of graphene on target substrates is feasible to achieve batch production of graphene wafers. In contrast with CVD method, the presence of C atoms in the substrate without a need for external source can make this process repeatable regardless of the size of the substrate and the synthesis quartz tube. Figure 4 shows 100 mm SiO_2 wafer covered with graphene. Raman spectroscopy was performed on several locations within the wafer to obtain average I_{2D}/I_G and I_D/I_G ratios. The comparison of Raman data for different locations demonstrates the high uniformity over the large area within one growth batch. Figures 4b and 4c show I_{2D}/I_G and I_D/I_G ratios obtained from Raman mapping performed on 60 µm by 60 µm area with a step size of 4 µm. Raman mapping of graphene verifies the uniformity on the microscale and suggests the excellent growth quality. Overall, this method results in uniformity of graphene better than the CVD approach after being transferred onto another substrate.

The impact of the Cu/Ni bilayer thickness on the growth of graphene was also studied. Different thicknesses of Cu and Ni were evaporated on SiO_2/Si substrates and the graphene synthesis was performed under the same condition as previously mentioned. Figure 5a shows I_{2D}/I_G and I_D/I_G ratios obtained from Raman measurements performed on samples with 150 nm thick Cu and different Ni thickness. Samples without Ni but only Cu did not result in formation of any graphene which is in accord with a previous report.[27] The sample with 1 nm Ni layer resulted in a defective graphene with a I_D/I_G ratio of 1.7 ± 0.05 and I_{2D}/I_G ratio of 1.1 ± 0.15. An increase in the Ni thickness to 10 nm resulted in a decrease in I_D/I_G to 0.2 ± 0.05 and increase in I_{2D}/I_G to 1.45 ± 0.05. Further increase in Ni thickness to 15 nm did not cause any notable difference in I_D/I_G and caused I_{2D}/I_G to decrease to 0.8 ± 0.2. Thicker Ni film can result in an excess amount of C in the Cu/Ni medium forming multilayer graphene. By controlling the thickness of the Ni layer with a fixed Cu layer, it is possible to control the quality of the synthesized graphene.

Next, the Ni layer was held constant and the impact of the Cu layer thickness on film growth was studied. The Ni only layer with 10 nm thickness resulted in a highly defective few-layer graphene film with an I_D/I_G ratio of 1.8 ± 0.2 and I_{2D}/I_G ratio of 1.1 ± 0.15. A sample with 10 nm thick Ni layer and Cu with different thicknesses of 150, 300, and 450 nm did not result in any notable change in the quality of synthesized film. Further increase in the Cu thickness was not tried as sufficient evaporation of the Cu layer, a key for this synthesis method, could not occur with thicker Cu films under the current synthesis conditions. Thus, fixing the Cu layer and modulating the Ni layer resulted in a better approach to controlling graphene film quality. Finally, graphene was grown on a quartz substrate using 150 nm thick Cu and 10 nm thick Ni. A Cary 5E UV-Vis-NIR dual-beam spectrophotometer was used to measure the optical transmittance from 400–2500 nm of the sample directly grown on the quartz substrate after wet etching treatment. An average transmittance ∼95% at 550 nm wavelength was observed as shown in Fig. 5b, suggesting that the sample synthesized through this technique consists of primarily bilayer graphene, as each layer absorbs between 2–2.5% at room temperature.[35] Raman spectroscopy measurements on the sample synthesized on quartz showed similar quality for graphene with an I_D/I_G ratio of 0.2 ± 0.05 and I_{2D}/I_G ratio of 1.45 ± 0.05 and indicated that our method does not depend on the growth substrate.

X-ray Photoelectron Spectroscopy was employed to identify the elements present on the sample surface before and after acid treatment. XPS data were acquired using a spectrophotometer (VG Scientific ESCALAB 210) with a Al Kα X-ray source ($h\upsilon$ = 1486.68 eV). The survey scan spectra were collected randomly at several points at the

Downloaded on 2013-05-16 to IP 128.61.142.206 address. Redistribution subject to ECS license or copyright; see ecsdl.org/site/terms_use

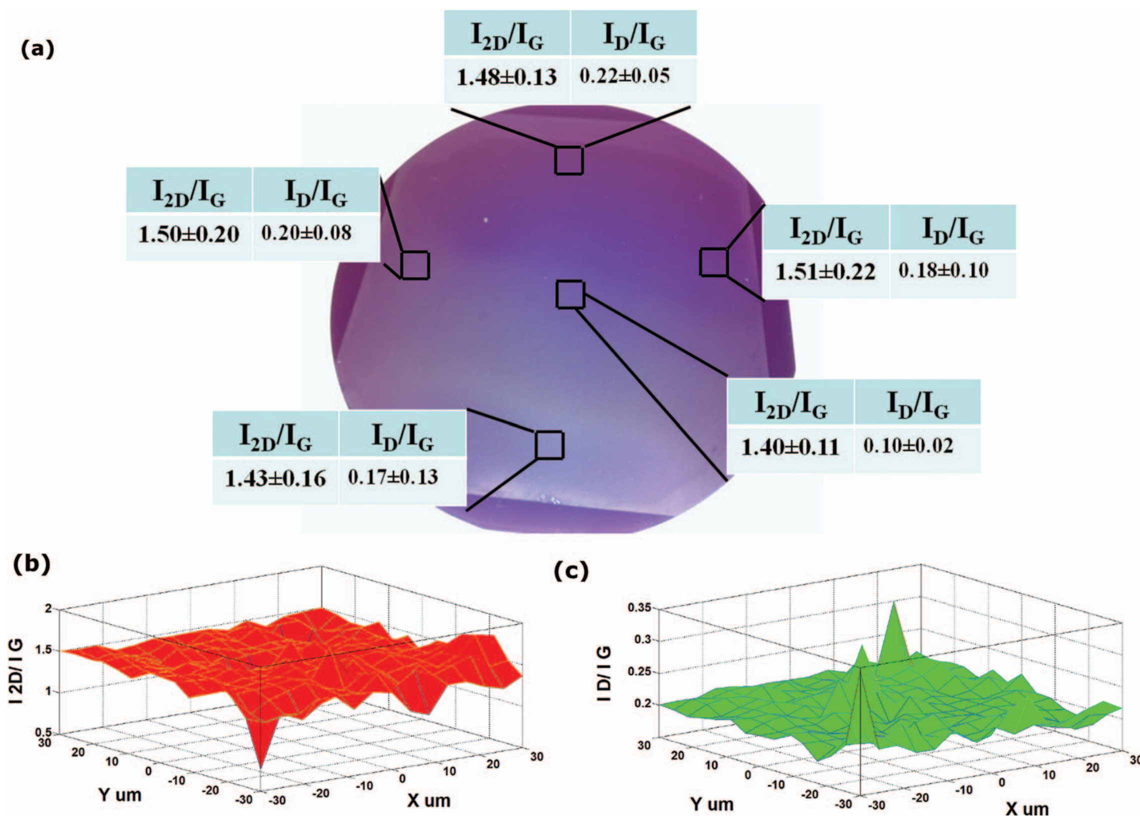

Figure 4. (a) 100 mm SiO_2 wafer covered with graphene. I_{2D}/I_G and I_D/I_G were obtained from the Raman measurements and averaged for each location indicative of high uniformity in macro scale within one growth batch. (b) and (c) I_{2D}/I_G and I_D/I_G obtained from Raman mapping performed on 60 μm by 60 μm area with 4 μm verifies the uniformity on the microscale.

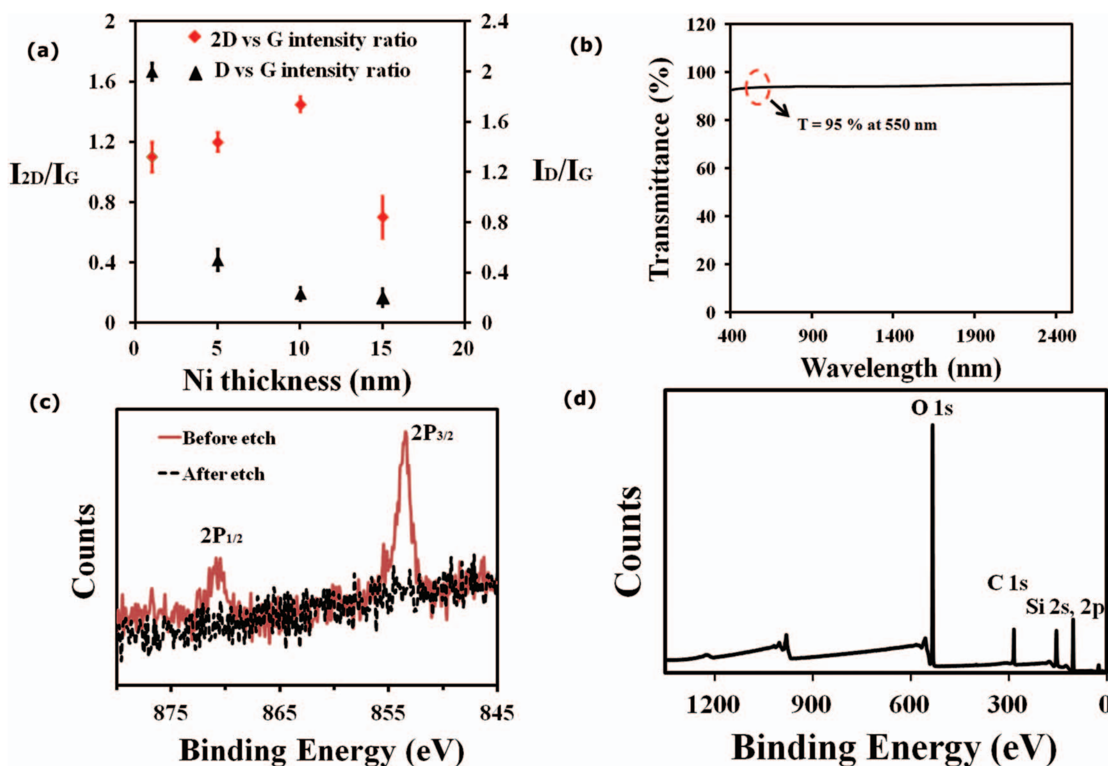

Figure 5. (a) I_{2D}/I_G and I_D/I_G obtained from the Raman measurements on samples with 150 nm thick Cu and different Ni thickness. (b) Average UV Vis spectra performed after wet etching indicates the synthesized graphene on quartz is primarily bi-layer showing ~95% transmittance at 550 nm. (c) Core level Ni XPS spectra shows removal of Ni after acid treatment. (d) Survey spectra collected randomly indicates the presence of C1s binding energy without any detectable peaks for Cu or Ni after wet etching.

Downloaded on 2013-05-16 to IP 128.61.142.206 address. Redistribution subject to ECS license or copyright; see ecsdl.org/site/terms_use

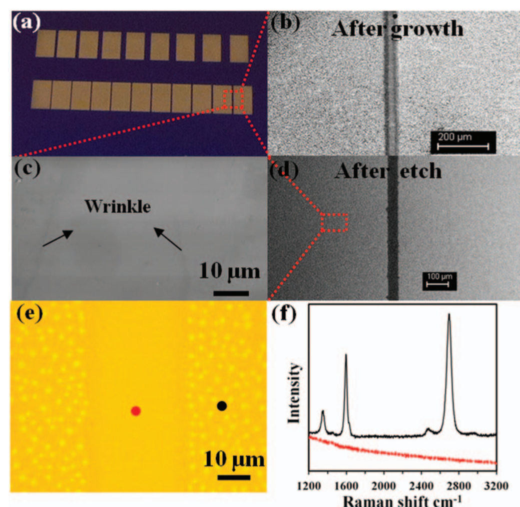

Figure 6. (a) Photograph of a typical patterned sample. (b) and (d) SEM image of the spacing before and after acid treatment. (c) SEM image of a graphene showing wrinkles. (e) Optical image of the spacing after growth. Showing presence of Cu dots. (f) Representative Raman spectra shows presence of graphene on the areas where Ni and Cu patterned. No graphitic peaks observed at other areas (in the spacing).

binding energy (B.E.) of 0–1300 eV with a step size of 1 eV at a pass energy of 200 eV and a spot size of 400 µm. High resolution XPS spectra of Ni was acquired over 845–880 eV with 400 µm spot size, 0.1 eV step size, and 50 eV pass energy. Comparison of Ni core level spectra before and after wet etching shown in Fig. 5c suggests that the acid treatment effectively removed all metals from the graphene film. The survey spectra prominently showed the C1s and O1s peaks and the lack of any peak associated with copper or nickel (see Fig. 5d). Oxygen was abundant on the surface, as XPS measurements were performed on the graphene that has been synthesized on the SiO_2 substrate.

To demonstrate the ability to perform patterned synthesis over a full wafer 100 mm wafer, a shadow mask used to selectively evaporate Ni and Cu on the substrate with a spacing down to 30 µm wide (see Fig. 6a). Then, the samples underwent the synthesis process described previously. Figures 6b and 6d show SEM images of the spacing before and after metal wet etching. A zoomed image of the graphene is shown in Fig. 6c. Raman spectroscopy was performed within the spacing and on the areas believed to have graphene. No evidence of graphene formation was seen in the spacing where the metals where not present. This indicates the ability to control and confine the synthesis of graphene layers to specific regions on the wafer surface without any post treatment patterning steps.

Conclusions

We report a new technique for producing large area, transfer-free graphene films on dielectric substrates using intrinsic carbon dissolved in bulk metals. By using a Ni and Cu bilayer film with large differences in C solubility, it is possible to force some of the dissolved carbon to the surface to form graphene layers. This method allows for the carbon source to be contained within the substrate and confine the growth of the graphene to areas where the bilayer metals are patterned. This method shows great potential for the direct synthesis of graphene on dielectric substrates, including low cost SiO_2/Si substrates where the integration with other microelectronics may be possible. Moreover, it can be scaled to batch processing of graphene over an entire wafer which may be important for the scalability of graphene manufacturing.

Acknowledgments

The authors are grateful for the support of Georgia Tech MRSEC and NSF CMMI grant number 0927736. The authors thank Walter Henderson and Gary Spinner at Georgia Tech Microelectronic Research Center for SIMS measurements and fruitful discussions.

References

1. K. S. Novoselov, A. K. Geim, S. V. Morozov, D. Jiang, Y. Zhang, S. V. Dubonos, I. V. Grigorieva, and A. A. Firsov, *Science*, **306**, 666 (2004).
2. K. S. Novoselov, A. K. Geim, S. V. Morozov, D. Jiang, M. I. Katsnelson, I. V. Grigorieva, S. V. Dubonos, and A. A. Firsov, *Nature*, **438**, 197 (2005).
3. C. Berger, Z. M. Song, X. B. Li, X. S. Wu, N. Brown, C. Naud, D. Mayou, T. B. Li, J. Hass, and A. N. Marchenkov et al., *Science*, **312**, 1191 (2006).
4. P. W. Sutter, J. I. Flege, and E. A. Sutter, *Nat. Mater.*, **7**, 406 (2008).
5. K. V. Emtsev, A. Bostwick, K. Horn, J. Jobst, G. L. Kellogg, L. Ley, J. L. McChesney, T. Ohta, S. A. Reshanov, and J. Rohrl et al., *Nat. Mater.*, **8**, 203 (2009).
6. D. Li, M. B. Muller, S. Gilje, R. B. Kaner, and G. G. Wallace, *Nat. Nanotechnol.*, **3**, 101 (2008).
7. G. Eda, G. Fanchini, and M. Chhowalla, *Nat. Nanotechnol.*, **3**, 270 (2008).
8. V. C. Tung, M. J. Allen, Y. Yang, and R. B. Kaner, *Nat. Nanotechnol.*, **4**, 25 (2009).
9. S. Stankovich, D. A. Dikin, G. H. B. Dommett, K. M. Kohlhaas, E. J. Zimney, E. A. Stach, R. D. Piner, S. T. Nguyen, and R. S. Ruoff, *Nature*, **442**, 282 (2006).
10. D. A. Dikin, S. Stankovich, E. J. Zimney, R. D. Piner, G. H. B. Dommett, G. Evmenenko, S. T. Nguyen, and R. S. Ruoff, *Nature*, **448**, 457 (2007).
11. X. L. Li, X. R. Wang, L. Zhang, S. W. Lee, and H. J. Dai, *Science*, **319**, 1229 (2008).
12. X. L. Li, G. Y. Zhang, X. D. Bai, X. M. Sun, X. R. Wang, E. Wang, and H. J. Dai, *Nat. Nanotechnol.*, **3**, 538 (2008).
13. Y. Hernandez, V. Nicolosi, M. Lotya, F. M. Blighe, Z. Y. Sun, S. De, I. T. McGovern, B. Holland, M. Byrne, and Y. K. Gun'ko et al., *Nat. Nanotechnol.*, **3**, 563 (2008).
14. K. S. Kim, Y. Zhao, H. Jang, S. Y. Lee, J. M. Kim, J. H. Ahn, P. Kim, J. Y. Choi, and B. H. Hong, *Nature*, **457**, 706 (2009).
15. A. Reina, X. T. Jia, J. Ho, D. Nezich, H. B. Son, V. Bulovic, M. S. Dresselhaus, and J. Kong, *Nano Lett.*, **9**, 30 (2009).
16. Q. K. Yu, J. Lian, S. Siriponglert, H. Li, Y. P. Chen, and S. S. Pei, *Appl. Phys. Lett.*, **93**, 113103 (2008).
17. X. S. Li, W. W. Cai, J. H. An, S. Kim, J. Nah, D. X. Yang, R. Piner, A. Velamakanni, I. Jung, and E. Tutuc et al., *Science*, **324**, 1312 (2009).
18. M. P. Levendorf, C. S. Ruiz-Vargas, S. Garg, and J. Park, *Nano Lett.*, **9**, 4479 (2009).
19. Z. Y. Juang, C. Y. Wu, C. W. Lo, W. Y. Chen, C. F. Huang, J. C. Hwang, F. R. Chen, K. C. Leou, and C. H. Tsai, *Carbon*, **47**, 2026 (2009).
20. J. Hofrichter, B. N. Szafranek, M. Otto, T. J. Echtermeyer, M. Baus, A. Majerus, V. Geringer, M. Ramsteiner, and H. Kurz, *Nano Lett.*, **10**, 36 (2010).
21. Z. Z. Sun, Z. Yan, J. Yao, E. Beitler, Y. Zhu, and J. M. Tour, *Nature*, **468**, 549 (2010).
22. S. J. Byun, H. Lim, G. Y. Shin, T. H. Han, S. H. Oh, J. H. Ahn, H. C. Choi, and T. W. Lee, *J. Phys. Chem. Lett.*, **2**, 493 (2011).
23. Z. C. Li, P. Wu, C. X. Wang, X. D. Fan, W. H. Zhang, X. F. Zhai, C. G. Zeng, Z. Y. Li, J. L. Yang, and J. G. Hou, *ACS Nano*, **5**, 3385 (2011).
24. J. M. Garcia, R. He, M. P. Jiang, P. Kim, L. N. Pfeiffer, and A. Pinczuk, *Carbon*, **49**, 1006 (2011).
25. L. M. A. Perdigao, S. N. Sabki, J. M. Garfitt, P. Capiod, and P. H. Beton, *J. Phys. Chem. C*, **115**, 7472 (2011).
26. M. S. Xu, D. Fujita, K. Sagisaka, E. Watanabe, and N. Hanagata, *ACS Nano*, **5**, 1522 (2011).
27. N. Liu, L. Fu, B. Dai, K. Yan, X. Liu, R. Zhao, Y. Zhang, and Z. Liu, *Nano Letters*, **11**, 297 (2011).
28. A. Ismach, C. Druzgalski, S. Penwell, A. Schwartzberg, M. Zheng, A. Javey, J. Bokor, and Y. G. Zhang, *Nano Lett.*, **10**, 1542 (2010).
29. C.-Y. Su, A.-Y. Lu, C.-Y. Wu, Y.-T. Li, K.-K. Liu, W. Zhang, S.-Y. Lin, Z.-Y. Juang, Y.-L. Zhong, F.-R. Chen, and L.-J. Li, *Nano Letters*, **11**, 3612 (2011).
30. Z. Peng, Z. Yan, Z. Sun, and J. M. Tour, *Acs Nano*, **5**, 8241 (2011).
31. Z. Yan, Z. Peng, Z. Sun, J. Yao, Y. Zhu, Z. Liu, P. M. Ajayan, and J. M. Tour, *Acs Nano*, **5**, 8187 (2011).
32. A. C. Ferrari, J. C. Meyer, V. Scardaci, C. Casiraghi, M. Lazzeri, F. Mauri, S. Piscanec, D. Jiang, K. S. Novoselov, and S. Roth et al., *Phys. Rev. Lett.*, **97**, 187401 (2006).
33. F. Tuinstra and J. L. Koenig, *J. Chem. Phys.*, **53**, 1126 (1970).
34. L. M. Malard, M. A. Pimenta, G. Dresselhaus, and M. S. Dresselhaus, *Phys. Rep.*, **473**, 51 (2009).
35. R. R. Nair, P. Blake, A. N. Grigorenko, K. S. Novoselov, T. J. Booth, T. Stauber, N. M. R. Peres, and A. K. Geim, *Science*, **320**, 1308 (2008).

Downloaded on 2013-05-16 to IP **128.61.142.206** address. Redistribution subject to ECS license or copyright; see **ecsdl.org/site/terms_use**